Journal Name

ARTICLE

Identification of a Common Recognition Center for a Photoactive Non-steroidal Antiinflammatory Drug in Serum Albumins of Different Species

Received 00th January 20xx,
Accepted 00th January 20xx

DOI: 10.1039/x0xx00000x

www.rsc.org/

Oscar Molins-Molina,[a] Emilio Lence,[b] Daniel Limones-Herrero,[a] Concepción González-Bello,[b] Miguel A. Miranda*[a] and M. Consuelo Jiménez*[a]

The non-steroidal anti-inflammatory drug (*S*)-carprofen (**CPF**) has been used as photoactive probe to investigate the possible existence of a common recognition center in serum albumins (SAs) of different species. The methodology involves irradiation of the **CPF**/SAs complexes, coupled with gel filtration chromatography or proteomic analysis of the photolisates, docking and molecular dynamic simulations. Photolysis of **CPF**/SAs complexes at λ = 320 nm, and gel filtration chromatography, the protein fraction still contained the drug fluorophore, in agreement with covalent attachment of the photogenerated radical intermediate **CBZ**$^{\bullet}$ to SAs. After trypsin digestion and ESI-MS/MS, incorporation of **CBZ**$^{\bullet}$ was detected at several positions in the different albumins. Remarkably, modifications at the IB/IIIA interface were observed in all cases (Tyr452 in HSA, RbSA and RtSA and Tyr451 in BSA, PSA and SSA). The molecular basis of this common recognition, studied by docking and Molecular Dynamics simulation studies on the corresponding non-covalent complexes, corroborated the experimentally observed covalent modifications. Our computational studies also revealed that the previously reported displacement of **CPF** by (*S*)-ibuprofen, a site II specific drug, would be due to an allosteric effect in site II, rather than a direct molecular displacement, as expected.

Introduction

Covalent photobinding of a ligand to a protein has recently been used as a tool for mapping the protein recognition center. This has been proven for a model system (carprofen methyl ester/bovine α_1 acid glycoprotein) using a systematic approach that combines photophysics, reactivity, proteomics and molecular dynamics simulation studies.[1]

The parent drug carprofen [2-(6-chloro-9H-carbazol-2-yl)propanoic acid] is a non-steroidal antiinflammatory drug (NSAID) of the 2-arylpropionic acids family employed for the treatment of pain and inflammation for almost a decade in the 90's. Then, it was removed from the market for human use, and currently tablets or injections are only used for veterinary purposes. It possesses a chiral center and the (*S*)-enantiomer is the pharmacologically active form (**CPF**, Chart 1).[2] Rather than glycoproteins, the major transport proteins for **CPF** are serum albumins (SAs), which are very abundant in mammals and play a crucial role in bio-distribution, metabolism and elimination of exogenous compounds.[3]

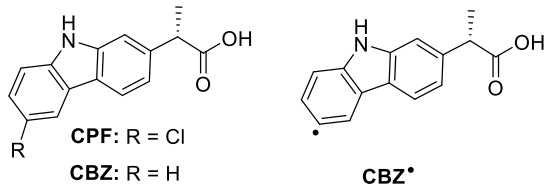

Chart 1. Chemical structures of (*S*)-carprofen (**CPF**), its photoreaction product (**CBZ**) and radical intermediate (**CBZ**$^{\bullet}$).

Human serum albumin (HSA) consists in a single polypeptide chain with a heart shaped three dimensional structure and three homologous domains I–III, each of them containing two sub-domains (A and B).[4] Small organic ligands bind to HSA in regions located within hydrophobic cavities of sub-domain IIA and IIIA.[5] While neutral, bulky heterocyclic compounds mostly bind to subdomain IIA by means of strong hydrophobic interactions, acidic molecules bind preferentially to subdomain IIIA, through electrostatic and/or H-bonding interactions.[6] The binding properties of other albumins, such as bovine, rabbit and rat serum albumins (BSA, RbSA and RtSA, respectively) have been explored using different techniques, such as high performance displacement chromatography, fluorescence or equilibrium dialysis.[7]

[a] *Departamento de Química/Instituto de Tecnología Química UPV-CSIC, Universitat Politècnica de València, Camino de Vera s/n, 46071 Valencia, Spain; E-mail: mcjimene@qim.upv.es*
[b] *Centro Singular de Investigación en Química Biolóxica e Materiais Moleculares (CIQUS), Departamento de Química Orgánica, Universidade de Santiago de Compostela, Jenaro de la Fuente s/n, 15782 Santiago de Compostela, Spain.*
Electronic Supplementary Information (ESI) available: See DOI: 10.1039/x0xx00000x

The *in vitro* supramolecular dark binding of **CPF** to HSA has been investigated by several methods, including photophysical techniques such as fluorescence and transient absorption spectroscopy.[8,9] The results show that although subdomain IIIA is the major binding site for **CPF** within HSA, subdomain IIA is also populated to some extent.

In contrast to the reversible, non-covalent complexation, photobinding corresponds to formation of a covalent photoadduct upon irradiation of a ligand in the presence of a protein. Photobinding is relevant to photoallergy, which is generally attributed to covalent conjugation of proteins with photosensitizing agents, photochemical intermediates or photoproducts (usually denoted as haptens); the resulting modified proteins can act as antigens, thus provoking the immune system response.[10] In this context, transport proteins, especially serum albumins, have been employed as models to investigate the photobinding process.[11]

In connection with the photoallergic properties of **CPF**,[12] its photobinding to HSA has been reported; the process is thought to involve formation of aryl radicals ($CBZ^{\cdot}$) resulting from C-Cl photocleavage and can be followed by incorporation of the fluorophore to the biomacromolecule.[8b,13] The process can be monitored by following the changes in the fluorescence band at increasing irradiation times, since the fluorescence quantum yield (ϕ_F) of resulting CBZ is much higher than that of parent **CPF**.

The analogies and differences between species in drug response are due to pharmacokinetic or pharmacodynamic aspects. Species differences are often unpredictable and generalizations are not easy to make. In the case of NSAIDs, some pharmacokinetic aspects (such as protein binding and distribution volumes) do not display significant variations between species, while others (i. e. clearance and elimination half-life) do. Concerning pharmacodynamic aspects, significant differences exist among animal species for this family of drugs, such as the relative potencies for inhibition of the COX-1 and COX-2 isoforms.[14]

In this context, the aim of the present work is to elucidate if there is a common recognition center for NSAIDs in SAs of different species, using the **CPF** as a photoactive probe for different SAs [human (HSA), bovine (BSA), porcine (PSA), rabbit (RbSA), rat (RtSA) and sheep (SSA)]. As a matter of fact, the combined information obtained from photoreactivity, proteomic and molecular dynamic simulation studies unambiguously demonstrated the existence of a common recognition center for **CPF** in SAs of the different species, in the interface between subdomains IB and IIIA.

Results and discussion

The obtained results are presented below, arranged under separate headings dealing with dark binding interactions, covalent photobinding and theoretical calculations.

Dark binding interactions in CPF/SA complexes

Non-covalent binding of **CPF** to SAs resulted in very subtle changes in the intensity and relative position of the **CPF** characteristic bands in the absorption spectra. Thus, shifts in the order of 3-5 nm were noticed in the spectra of 1:1 complexes (**CPF**/SA) respect to those obtained by addition of independent drug and protein contributions (**CPF**+SA) (Table 1). The set of spectra for all the SAs is presented in Figure S1 of the SI.

Table 1. Photophysical data on **CPF**/SAs complexes

Complex	$\Delta\lambda_1$,$\Delta\lambda_2$[a]	τ_T[b]	I_F[c]
CPF/HSA	3, 4	9.3	1.0
CPF/BSA	3, 5	15.7	0.8
CPF/PSA	3, 3	12.4	1.4
CPF/RbSA	3, 5	6.4	2.0
CPF/RtSA	4, 5	10.6	2.2
CPF/SSA	3, 4	16.1	1.0

[a] Shifts of the position of characteristic absorption bands in **CPF**/SA respect to **CPF**+SA, in nm; $\Delta\lambda_1$ correspond to the band at *ca*. 270 nm and $\Delta\lambda_2$ to the band at *ca*. 305 nm; [b] average triplet lifetime, at λ_{exc} = 355 nm, under air, in microseconds. The value in the absence of protein is lower than 1 μs. [c] Relative fluorescence intensity (λ_{exc} = 320 nm) at the maxima for irradiated **CPF**/SAs, after Sephadex filtration, taking **CPF**/HSA as reference.

Laser flash photolysis was performed at λ_{exc} = 355 nm for **CPF**/SAs. Complexation was evidenced by lengthening (by one order of magnitude) of triplet excited state decays (^{3}**CPF***) monitored at λ = 450 nm in the presence of SAs (Table 1 and Figure 1).

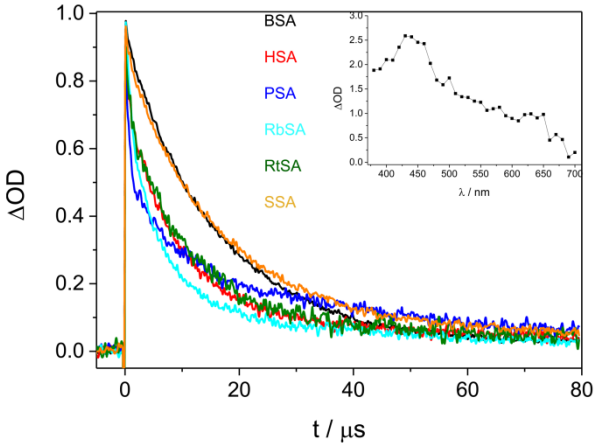

Figure 1. Laser flash photolysis of **CPF** ([**CPF**] = 10^{-4} M, λ_{exc} = 355 nm, PBS, air) in the presence of different SAs at 1:1 drug/protein molar ratio. Decays monitored at λ = 450 nm. Inset. Transient absorption spectra of **CPF**/HSA 1.4 μs after the laser shot.

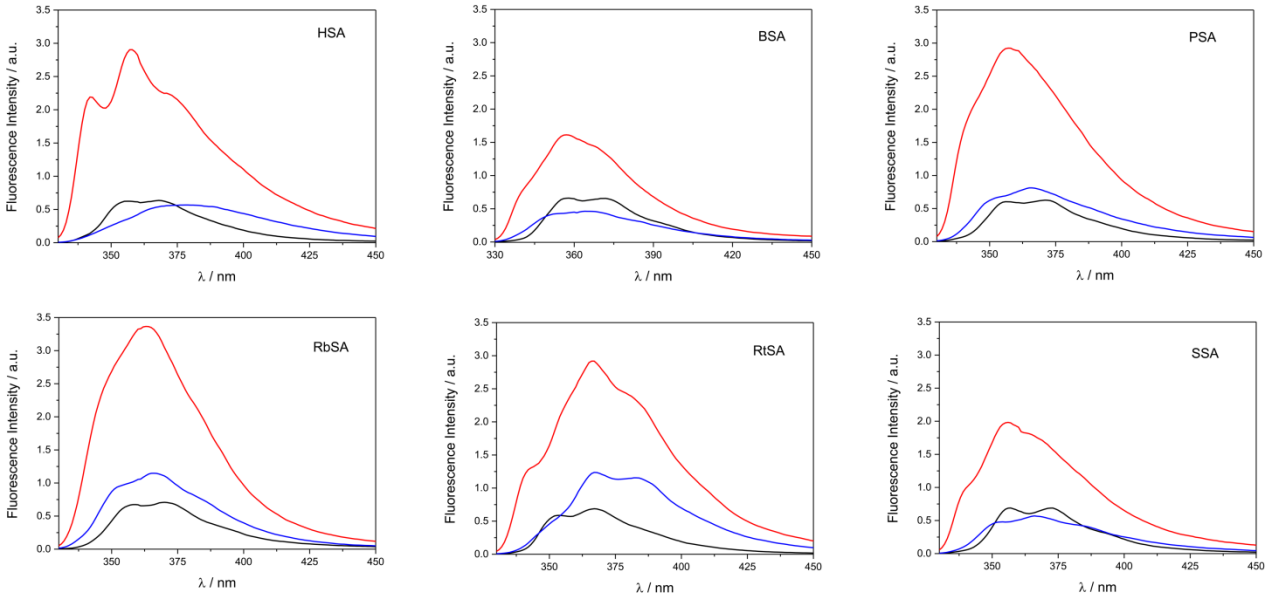

Figure 2. Fluorescence spectra of CPF/SA mixtures at 1:1 drug/protein molar ratio: before irradiation (black trace), after 3 min of irradiation at λ_{exc} = 320 nm (red trace) and after Sephadex filtration of the photolyzate (blue trace).

Covalent drug-protein photobinding

Solutions of **CPF**/SA (1:1 molar ratio) were irradiated at λ = 320 nm. The spectra recorded before (black traces) and after 3 minutes of irradiation (red traces) are shown in Figure 2. In general, the emission bands of the irradiated samples were more intense. This is in agreement with the occurrence of photodehalogenation, leading to products with a ϕ_F much higher than that of **CPF**.[15]

To check whether covalent modification of the proteins was occurring, the photolysates were treated with 6M of guanidinium chloride and filtered through Sephadex (see experimental details in the SI), a process that allows removing the species of low molecular weight. The obtained spectra are also shown in Figure 2 (blue traces). In general, filtration through Sephadex was associated with a remarkable decrease of the emission intensity (compare red and blue traces), indicating that an important fraction of the generated photoproducts was not bound to the protein. Nonetheless, emission was still clearly observed, demonstrating that **CPF**-derived species are covalently attached to the SAs. In parallel, non-irradiated samples of **CPF**/SAs were subjected to the same work up, as control experiments; as expected from the lack of covalently bound adducts, no emission was observed in these cases. The extent of photobinding relative to the **CPF**/HSA system is given in Table 1.

Having demonstrated the photobinding of **CPF** to the SAs by gel filtration chromatography coupled with fluorescence measurements, the formation of covalent photoadducts was investigated in more detail by proteomic analysis. These studies were expected to provide precise information of which amino acid(s) are covalently modified. Thus, the photoreactivity of **CPF** with the six SAs was addressed. The irradiated **CPF**/SAs systems were filtered to remove excess of ligand; then, trypsin or endoproteinase Glu-C digestions were followed by HPLC-MS/MS. This was intended to obtain information on the modified peptide sequence and to characterize the adduct. Full scan and fragmentation data files were analyzed by using the Mascot® database search engine (Matrix Science, Boston, MA, USA) and by entering variable modifications that take into account the main possible residues (FWY) able to react with the carbazolyl radical **CBZ•** obtained after dehalogenation of **CPF**.

For the human protein, the main results confirmed identification of **CBZ**-HSA derived peptide adducts at Phe134, Trp214 and Tyr452 (Figure 3 and Table 2), according to the ESI-MS/MS spectra and fragmentation pattern of the modified peptides, that agreed well with the “y” and “b” ion series (see pages S3-S5 in the SI).

```
  1 MKWVTFISLL FLFSSAYSRG VFRRDAHKSE VAHRFKDLGE ENFKALVLIA
 51 FAQYLQQCPF EDHVKLVNEV TEFAKTCVAD ESAENCDKSL HTLFGDKLCT
101 VATLRETYGE MADCCAKQEP ERNECFLQHK DDNPNLPRLV RPEVDVMCTA
151 FHDNEETFLK KYLYEIARRH PYFYAPELLF FAKRYKAAFT ECCQAADKAA
201 CLLPKLDELR DEGKASSAKQ RLKCASLQKF GERAFKAWAV ARLSQRFPKA
251 EFAEVSKLVT DLTKVHTECC HGDLLECADD RADLAKYICE NQDSISSKLK
301 ECCEKPLLEK SHCIAEVEND EMPADLPSLA ADFVESKDVC KNYAEAKDVF
351 LGMFLYEYAR RHPDYSVVLL LRLAKTYETT LEKCCAAADP HECYAKVFDE
401 FKPLVEEPQN LIKQNCELFE QLGEYKFQNA LLVRYTKKVP QVSTPTLVEV
451 SRNLGKVGSK CCKHPEAKRM PCAEDYLSVV LNQLCVLHEK TPVSDRVTKC
501 CTESLVNRRP CFSALEVDET YVPKEFNAET FTFHADICTL SEKERQIKKQ
551 TALVELVKHK PKATKEQLKA VMDDFAAFVE KCCKADDKET CFAEEGKKLV
601 AASQAALGL
```

Figure 3. Amino acid sequence of HSA, with the amino acids modified by covalent binding of **CBZ** indicated in red.

Table 2. Modified peptides in HSA, with experimental and calculated mass values

Peptide	Mr exp	Mr calc[a]
LVRPEVDVMCTAFHDNEETFLKK	3014.4445	3014.4306
AFKAWAVAR	1255.6516	1255.6502
DYLSVVLNQLCVLHE	2037.9448	2037.9870

[a] Monoisotopic mass of peptide

The procedure was performed for the whole set of investigated proteins. The observed modified amino acids are indicated in Table 3; the protein sequence with the modified amino acids highlighted together with the ESI-MS/MS spectra and fragmentation pattern of all the peptide sequences are presented in pages S6-S28 of the SI. Remarkably, for the six homologous proteins, covalent modification of the tyrosine residue located at the interface between sub-domain IB and IIIA was obtained (Tyr452 for HSA).

Table 3. Summary of the experimentally observed covalent modifications in diverse homologous serum albumins[a,b,c]

Binding pocket	HSA	BSA	PSA	RbSA	RtSA	SSA
IB	Phe134	Tyr137		Phe134 Tyr138 Phe149	Phe134 Tyr138, Phe149 Tyr161	Tyr137
IIA	Trp214			Tyr291		
IIB		Phe325 Phe329			Phe330	Phe325 Phe329
IB/IIIA interface	Tyr452	Tyr451	Tyr451	Tyr452	Tyr452	Tyr451
IIIB		Phe508	Phe550		Phe509	

[a] Only non-external modifications are considered. [b] The modifications are organized according to the binding pocket. [c] The indicated numbering is the one used in the available crystallographic structures where the position of the first 24 amino acids is not resolved.

A plausible mechanism for the photomodification of SAs is depicted in Scheme 1. It involves reaction of ^{3}**CPF*** with Trp to afford the corresponding radical ion pairs; the CBZ radical formed after loss of Cl^- would react with Phe, Tyr or Trp resulting in covalent binding to these residues.

Molecular modelling studies

For the six homologous proteins the covalent modification of the tyrosine residue located in helix h4-III[16] of sub-domain IIIA was obtained (Tyr452 for HSA). This suggested that the main binding pocket of **CPF** is the interface region of sub-domains IIIA and IB, in which the tyrosine residue is located (Figure 4A). The latter residue is placed on the cleft of the serum albumin "V" structure and about 10 Å away from Trp214 (in HSA). Another relevant binding pocket of **CPF** to serum albumins, which was identified in four of the six proteins, is the most accessible part of sub-domain IB involving helix h7-I, h8-I, h9-I and h10-I (Figure 4B). Moreover, with the exception of HSA and PorSA, binding to the pocket composed by helix h7-II, h8-II and h9-II in sub-domain IIB was identified (Figure 4B). The proteomic results also showed that for HSA, as well as RbSA protein, binding to site I (sub-domain IIA) takes place.

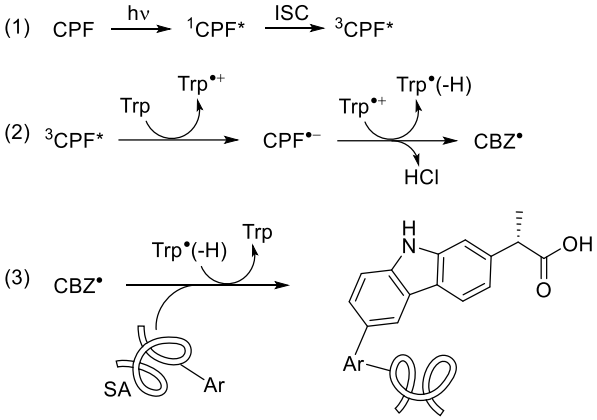

Scheme 1. Proposed covalent modification mechanism.

In order to get a better understanding of the binding interactions responsible for the affinity of **CPF** to SA proteins, the binding mode of this compound in atomic detail was explored. These studies were focused on HSA and on the main binding pockets identified by the proteomic studies: (i) "V" cleft between domains I and II; and (ii) sub-domain IB (Figure 4). To this end, molecular docking using GOLD 5.2.2[17] program and the protein coordinates found in the crystal structure of HSA in complex with palmitic acid (PDB code 4BKE,[18] 2.35 Å) was first used. This structure was chosen because contains ligand molecules (palmitic acid) in some of the regions studied in this work and has higher resolution than other HSA structures. The proposed binding mode was further analysed by Molecular Dynamics (MD) simulation studies in order to assess the stability and therefore the reliability of the postulated binding. The results of these studies in the three pockets are discussed below.

Binding to "V" cleft pocket. Our MD simulation studies revealed that the binary **CPF**/HSA-V cleft complex is very stable, confirming the reliability of the proposed binding. Thus, an analysis of the root-mean-square deviation (rmsd) for the three domains of protein backbone (Cα, C, N and O atoms) calculated for the complex obtained from MD simulation studies (150–200 ns) revealed that it varied slightly, in particular for sub-domains IIIA (0.6 to 1.9 Å) and IB (0.9 to 1.2 Å) that surround the ligands (Figure S3). As expected, the more flexible part of the complex showed to be sub-domain IIIB, which is the one of the most accessible sub-domains of the protein that in the absence of ligand bounded undergoes conformational changes up to 10 Å.[19] Moreover, at the beginning of the simulation (the first ~30 ns) a small displacement of the ligand was observed resulting from the

initial adjustment of a large ligand into the structure. But eventually the ligand revealed to be stable during most of the simulation (~170 ns). Considering the high sequence similarity of the studied serum albumins in general, and of the "V" cleft in particular (Figure S2), we believe that the proposed binding mode of **CPF** for HSA would be quite similar for the other homologous proteins.

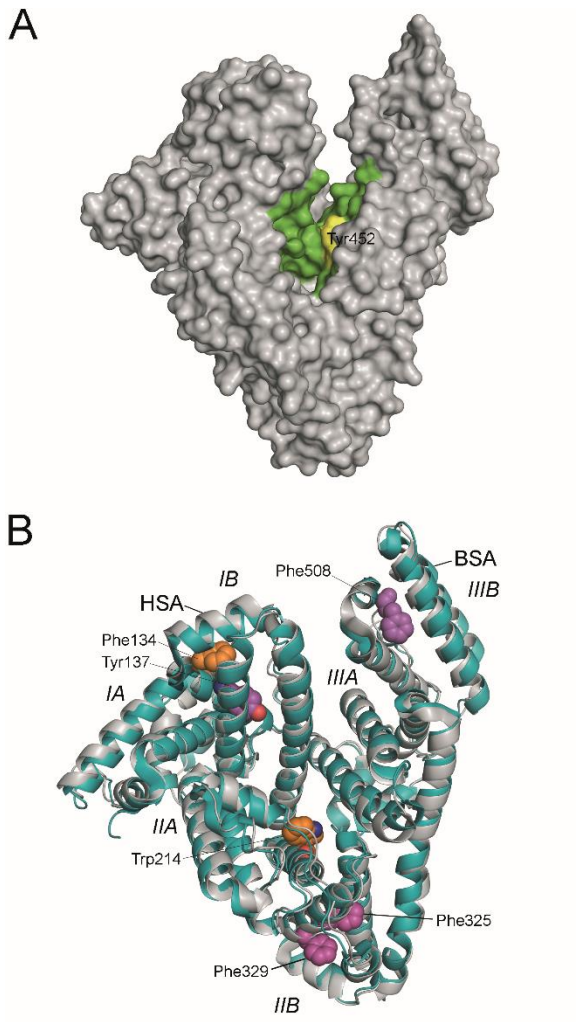

Figure 4. Determined binding pockets of carprofen to serum albumin proteins. (A) Main recognition pocket that is located in the cleft of the serum albumin "V" structure (green) involving the interface region between sub-domains IIIA and IB. The experimentally observed modified residue is highlighted in yellow. The structure corresponds to wild-type HSA (PDB 1E7B). (B) Other relevant binding pockets observed in two of the proteins studied. The crystal structures of HSA (PDB 1E7B, grey) and BSA (PDB 3V03, blue) are compared showing the determined pockets and the modified residues as spheres (orange for HSA and purple for BSA). The sub-domains of serum albumins are also labeled.

As Figure 5 shows, **CPF** would be anchored to the "V" cleft pocket through its carboxylate group through strong electrostatic interactions with the guanidinium group of Arg114 and the ε-amino group of Lys190 and a strong hydrogen bonding between the NH group of its aromatic moiety and the side chain carbonyl group of Asn429. In addition, the aromatic ring is stabilized by numerous lipophilic interactions with the apolar residues that surround it involving residues Ala191, Ala194, Val433, Val455, Val456, Val426 and Gln459. Under this arrangement, the C4 carbon atom attached to the chlorine atom in **CPF** would be located pointing towards the side chain of Tyr452, which is the only aromatic residue in the vicinity of the ligand. The proposed binding mode would explain therefore the experimentally observed covalent modification of Tyr452.

It was previously suggested that **CPF** binds with high affinity to site II and with weaker affinity to site I on HSA.[20] This was corroborated with diverse competition studies with site specific drugs such as (*S*)-ibuprofen (IBU, site II) and warfarin (site I). As it would be discussed below, the proteomic and molecular modelling studies reported here also corroborate site I as a secondary binding site of **CPF**. However, our results clearly showed that the main binding pocket of **CPF** is the cleft of the serum albumin "V" structure and not site II, as no covalent modifications of the aromatic residues of this pocket were observed in any of the six proteins studied. Reasoning that: (1) as observed in the crystal structure of HSA in complex with two molecules of ibuprofen (PDB code 2BXG,[21] 2.7 Å), this cleft is located nearby to site II; and (2) the significant conformational changes that HSA can undergo upon binding ligands, specifically in domains I and III, as previously reported by Curry *et al*[22] and also by us[19], we considered that the experimentally observed displacement of **CPF** by ibuprofen, which suggest site II as the main binding pocket, is also in agreement with the herein proposed binding. Thus, we believe that the higher affinity of ibuprofen than **CPF** to HSA and the expected conformational changes resulting of ibuprofen binding, in particular in the proximity of site II, might disfavor the binding of **CPF** to the "V" cleft of the protein. As a consequence, **CPF** would be displaced from its main binding pocket by an allosteric effect in site II, rather than a molecular displacement. In order to corroborate this allosteric modulation hypothesis, the conformational changes that **CPF**/HSA complex undergoes upon ibuprofen binding were studied by MD simulation studies. To this end, **CPF** was manually docked into the "V" cleft of the tertiary IBU/HSA complex (PDB code 2BXG) with the arrangement observed in the binary **CPF**/HSA complex (Figure 5B) and the resulting quaternary complex was subjected to 100 ns of MD simulation. The opposite case was also explored, i.e. the addition of two molecules of ibuprofen to the binary **CPF**/HSA complex, providing similar results. Whereas no significant changes were observed in the binding mode of the two ibuprofen molecules (*S*-isomer), which remain stable during the whole simulation (Figures 6A and 6B), **CPF** underwent a large displacement from its original binding pocket (up to 15 Å) as well as significant variations in its binding arrangement (rotation) as a consequence of the loss of its main anchoring interactions (Figure 6C). This is clearly visualized by comparison of its position in the binary **CPF**/HSA complex and after 100 ns of dynamic simulation in the quaternary IBU+IBU+**CPF**/HSA complex (Figure 6D). The binding free energy calculated for each ligand in their corresponding pockets of the complex also highlighted the lower binding affinity of **CPF** (Table 4, entries 3

vs 1). This was calculated using the MM/PBSA[23] approach in implicit water (generalised Born, GB) as implemented in Amber. Thus, whereas the affinity of ibuprofen to both pockets is retained or even increased, a large decrease on the calculated binding free energy of **CPF** is predicted (~ 6.8 kcal).

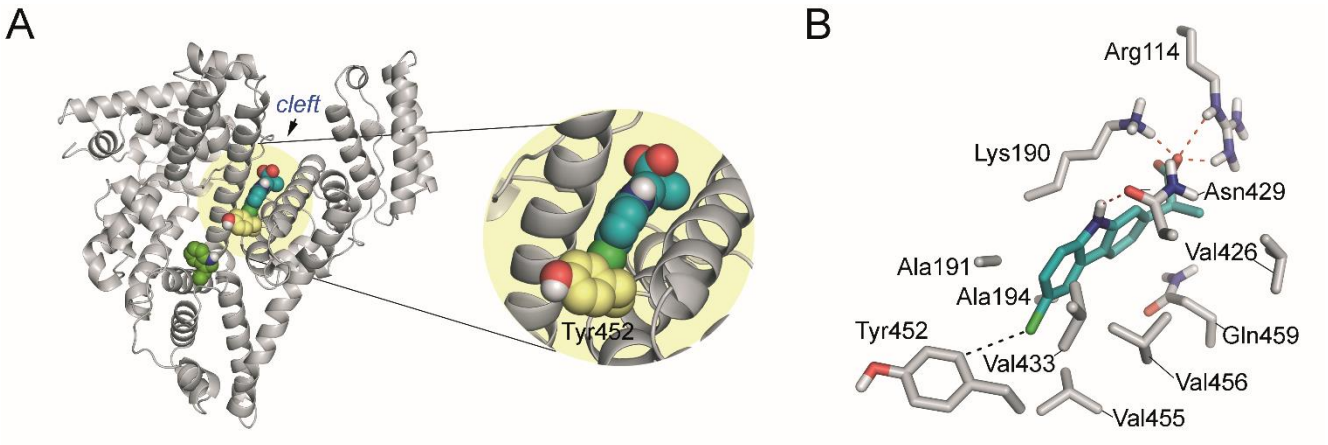

Figure 5. (A) Overall view of the proposed binary **CPF**/HSA-V cleft complex obtained by docking and MD simulation studies. An Snapshot after 150 ns is shown. (B) Detailed view of the **CPF**/HSA-V cleft complex. Relevant side chain residues are shown and labelled. Polar (red) contacts and distances (black) to Tyr452 are shown as dashed lines.

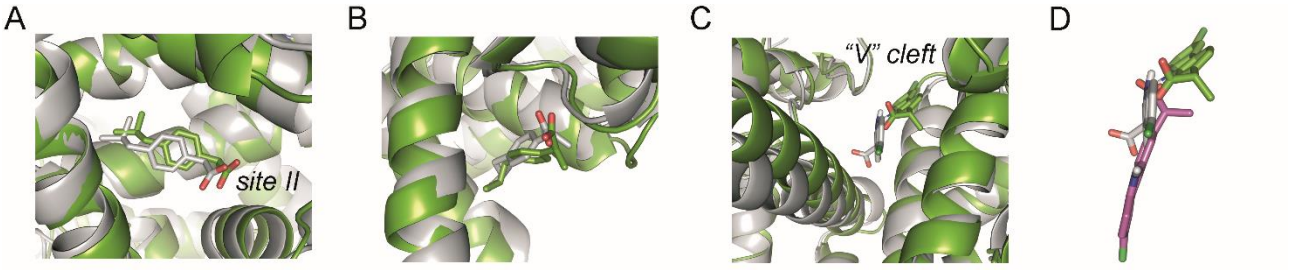

Figure 6. (A-C) Comparison of the quaternary IBU+IBU+**CPF** HSA/ complex after minimisation and prior to simulation (grey) and after 100 ns of dynamic simulation (green). A close view of IBU (A and B) and **CPF** (C) binding sites is provided. (D) Comparison of the position of **CPF** in the binary **CPF/**HSA/ complex (see Fig. 5B) and in the quaternary one (A−C). Note how whereas for IBU no significant changes are observed during the simulation, **CPF** is displaced from its binding pocket even prior to simulation.

Table 4. Calculated Binding Free Energies using MM/PBSA of diverse HSA/ligand(s) complexes to distinct pockets of the protein.

Entry	Complex	Ligand(s)	*"V" cleft*	*sub-domain IB*	*site II*	*sub-domain IIB*
1	Binary	**CPF**	−28.5 ± 0.4[a]			
2		**CPF**		−37.5 ± 0.2[a]		
3	Quaternary	IBU (×2) + **CPF**	−21.7 ± 0.2[a]		−40.8 ± 0.5[a]	−40.6 ± 0.2[a]

[a] standard error of mean.

Binding to sub-domain IB. The results of proteomic studies revealed also that **CPF** binds to sub-domain IB. In all serum albumin proteins, this is a pocket rich in phenylalanine and tyrosine residues and, even in some cases it is composed by a tryptophan residue (Trp158 in PSA, SSA and BSA). It recognizes compounds such as palmitic acid (PDB code 4BKE[18]), bicalutamide (PDB code 4LA0[24]) and hemin (PDB code 1O9X[25]). Our computational studies revealed that **CPF** would be anchored to HSA pocket through an electrostatic interaction of its carboxylate group with the guanidinium group of Arg117 and a hydrogen bonding with the phenol group of Tyr161 (Figure 7). In addition, the aromatic moiety of the ligand would have favorable lipophilic interactions with diverse residues, specifically, Leu115, Met123, Leu135, Tyr138, Tyr161, Phe165, Leu182, and the carbon side chain of Lys162. No interactions for the NH group of the ligand were identified. Under this arrangement, the experimentally observed modified Phe134 would be the closest aromatic residue to the chlorine atom of

the ligand (Figure 7B). Moreover, the binding free energies calculated predicted a high affinity for this pocket (Table 4, entry 2). An analysis of rmsd for the three domains of protein backbone (Cα, C, N and O atoms) calculated for the complex obtained from MD simulation studies revealed that it is very stable (Figure S4).

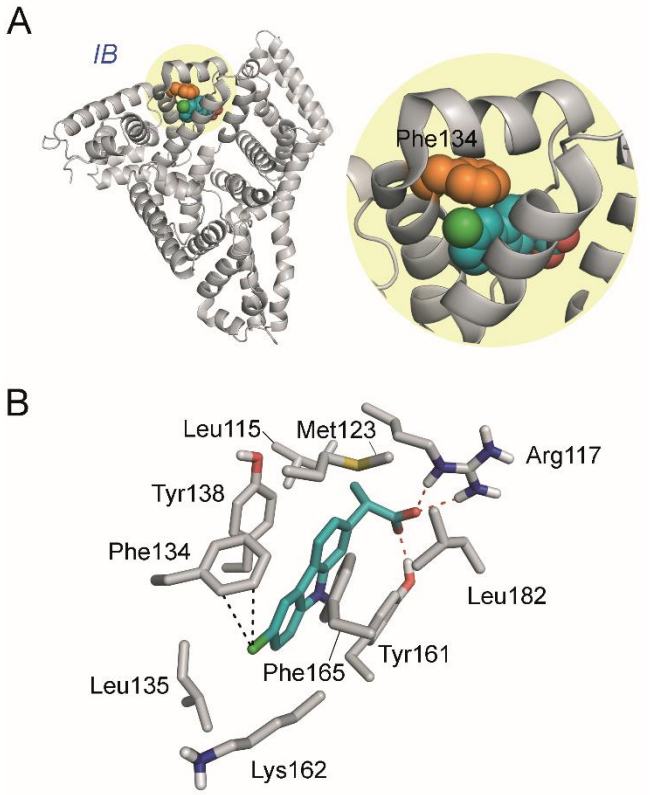

Figure 7. (A) Overall view of the binary **CPF**/HSA-IB complex obtained by docking and MD simulation studies. The ligand and residue modified are shown as spheres. (B) The viewpoint showed corresponds to snapshot after 50 ns of MD simulation. Relevant side chain residues are shown and labelled. Polar (red) contacts and distances (black) to Phe134 are shown as dashed lines.

Conclusions

In the dark, **CPF** binds to serum albumins of different species, giving rise to non-covalent complexes. These complexes show characteristic features in their photophysical properties, being especially noteworthy the lengthening of their triplet excited state lifetimes by at least one order of magnitude. Irradiation of the complexes by selective excitation of the **CPF** chromophore leads to irreversible covalent binding, as demonstrated by gel filtration chromatography, where incorporation of the fluorophore to the protein fraction is clearly observed. Digestion of the irradiated **CPF**/SAs complexes and subsequent proteomic analysis reveal attachment of the photodehalogenated drug to selected amino acid residues. Remarkably in all the investigated proteins, covalent modification of Tyr452 (in HSA, RbSA, RtSA) or Tyr451 (in BSA, PSA, SSA) is consistently observed. This indicates the presence of a common recognition center in SAs, irrespective of the involved species, at the interface between sub-domains IB and IIIA ("V" cleft pocket). Another relevant binding pocket of **CPF** to serum albumins, which was identified in four of the six proteins, proved to be the most accessible part of sub-domain IB.

The molecular basis of this common recognition was studied by Molecular Dynamics simulation studies of the corresponding non-covalent complexes. The results revealed that these complexes are very stable and the carbon atom of **CPF** in which the radical is generated, would be in close contact with the identified aromatic residues. Moreover, diverse previously reported competition studies with site specific drugs such as (*S*)-ibuprofen (site II) and warfarin (site I) revealed that **CPF** binds with high affinity to site II and with weaker affinity to site I on HSA. The proteomic and molecular modelling studies reported here also corroborate this idea. Our studies revealed that **CPF** would be displaced by (*S*)-ibuprofen from its main binding pocket by an allosteric effect in site II, rather than an expected direct molecular displacement. The former would be due to: (i) the large conformational changes that HSA can undergo upon binding ligands, and (ii) the close proximity of this cleft to site II. The reported integrated strategy that involves irradiation of **CPF**/SA complexes, coupled with fluorescence, identification of the photoinduced modified amino acid residues by proteomic analysis, docking and MD simulation studies could, in principle, be extended to a variety of protein/ligand complexes if an active chromophore is present in the ligand.

Experimental

General

Racemic carprofen, **HSA**, **BSA**, **PSA**, **RbSA**, **RtSA** and **SSA** were commercially available. Spectrophotometric, HPLC or reagent grade solvents were used without further purification. Solutions of phosphate-buffered saline (PBS) (0.01 M, pH 7.4) were prepared by dissolving phosphate-buffered saline tablets in Milli-Q water. Steady state absorption spectra were recorded in a JASCO V-630 spectrophotometer. Analytic HPLC analysis was performed by means of a Waters HPLC system connected to a PDA Waters 2996 detector. HPLC isolation was carried out on a JASCO HPLC equipment, composed of a DG-2080-54 degasification system, LG-2080-04 mixer and a PU-2080 pump connected to a UV-1575 detector. The (S)-enantiomer of carprofen was separated from a 1.8 M racemic mixture in methyl *tert*-butyl ether by HPLC (Technocroma Kromasil 100-TBB column, mobile phase hexane/methyl *tert*-butyl ether/acetic acid (45:55:0.1, v/v/v) flow 2.2 mL/min

Fluorescence Experiments

Spectra were recorded on a JASCO FP-8500 spectrofluorometer system, provided with a monochromator in the wavelength range of 200–850 nm, at 22 °C. Experiments were performed on solutions of **CPF** (2.5×10^{-5} M) in the presence of SAs (at 1:1 **CPF**/SA), employing 10 × 10 mm^2 quartz cells with 4 mL capacity. Excitation wavelength was 320 nm.

Laser Flash Photolysis Experiments

A Q-switched Nd:YAG laser (Quantel Brilliant, 355 nm, 15 mJ per pulse, 5 ns fwhm) coupled to a mLFP-111 Luzchem miniaturized equipment was employed. This transient absorption spectrometer includes a ceramic xenon light source, 125 mm monochromator, Tektronix 9-bit digitizer TDS-3000 series with 300 MHz bandwidth, compact photomultiplier, power supply, cell holder and fiber optic connectors, fiber optic sensor for laser-sensing pretrigger signal, computer interfaces, and a software package developed in the LabVIEW environment from National Instruments. The LFP equipment supplies 5 V trigger pulses with programmable frequency and delay. The rise time of the detector/digitizer is ~3 ns up to 300 MHz (2.5 GHz sampling). The monitoring beam is provided by a ceramic xenon lamp and delivered through fiber optic cables. The laser pulse is probed by a fiber that synchronizes the LFP system with the digitizer operating in the pretrigger mode. Transient spectra and kinetic traces were recorded employing 10×10 mm^2 quartz cells with 4 mL capacity. The concentration of **CPF** was 1.0 $\times 10^{-4}$ M, and the **CPF**/SA molar ratio was 1:1. All the experiments were carried out at room temperature. The $<\tau_T>$ values of **CPF** were determined by fitting the decay traces at λ_{max} = 450 nm by means of a monoexponential function.

Steady-State Photolysis Experiments

Steady-state photolysis of **CPF** (2.5×10^{-5} M) was performed by using a 150 W Xe lamp coupled to a monochromator at lamp output (λ_{exc} = 320 nm) in PBS under air and in the presence of protein (**CPF**/SA 1:1 molar ratio), through Pyrex. The course of the reaction was followed by monitoring the changes in the fluorescence spectra of the reaction mixtures at increasing times.

Treatment with Guanidinium Chloride and Filtration through Sephadex

Guanidinium chloride (1.72 mL, 6 M) was added to 3 mL of **CPF**/SA in PBS, in order to cause protein denaturation. The mixture was then filtered through a Sephadex P-10 column. Firstly, 25 mL of pure PBS were eluted; then 2.5 mL of the **CPF**/SA mixture treated with GndCl were eluted. Subsequently, 3.5 mL of PBS were eluted again. The absorption and emission of the final sample were then measured. To take into account the dilution factor, a similar experiment was conducted directly on SA (in the absence of **CPF**). In this way, the ratio between the absorbance value before and after filtration was obtained, which was employed as correction factor in the experiments.

Protein Digestion and LC-ESI-MS/MS Analysis

After irradiation, the SAs were enzymatically digested into smaller peptides using trypsin or V8. Subsequently, these peptides were analyzed using nanoscale liquid chromatography coupled to tandem mass spectrometry (nano LC-MS/MS). Briefly, 20 µg of sample were taken (according to Qubit quantitation) and the volume was set to 20 µL. Digestion was achieved with sequencing grade trypsin (Promega) or Glu-C. For the case of trypsin, the steps are: i) 2 mM DTT in 50 mM NH_4HCO_3 V = 25 µL, 20 min (60 °C); ii) 5.5 mM IAM in 50 mM NH_4HCO_3 V = 30 µL, 30 min (dark); iii) 10 mM DTT in 50 mM NH_4HCO_3 V = 60 µL, 30 min; iv) Trypsin (Trypsin: Protein ratio 1:20 w/w) V = 64 µL, overnight 37 °C. Digestion was stopped with 7 µL 10% TFA (Cf protein ca 0.28 µg/µL). Next, 5 µL of sample (except the main bands) were loaded onto a trap column (NanoLC Column, 3µ C18–CL, 350 um x 0.5 mm; Eksigent) and desalted with 0.1% TFA at 3 µL/min during 5 min. The peptides were then loaded onto an analytical column (LC Column, 3 µ C18–CL, 75 um × 12 cm, Nikkyo) equilibrated in 5% acetonitrile 0.1% formic acid. Elution was carried out with a linear gradient of 5 to 45% B in A for 30 min (A: 0.1% formic acid; B: acetonitrile, 0.1% formic acid) at a flow rate of 300 µL/min. Peptides were analyzed in a mass spectrometer nanoESI qQTOF (5600 TripleTOF, ABSCIEX). The tripleTOF was operated in information-dependent acquisition mode, in which a 0.25-s TOF MS scan from 350–1250 m/z was performed, followed by 0.05-s product ion scans from 100-1500 m/z on the 50 most intense 2−5 charged ions. ProteinPilot v4.5. (ABSciex) search engine default parameters were used to generate peak list directly from 5600 TripleTOF wiff files. The obtained mgf was used for identification with MASCOT (v 4.0, Matrix- Science). Database search was performed on SwissProt database. Searches were done with tryptic specificity allowing one missed cleavage and a tolerance on the mass measurement of 100 ppm in MS mode and 0.6 Da in MS/MS mode. Carbamidomethylation of Cys was used as a fixed modification and oxidation of Met and deamidation of Asn and Gln as variable modifications. A modification was defined in Phe, Tyr, Trp for **CPF**.

Docking Studies

They were carried out using program GOLD 5.2.2[17] and the protein coordinates found in the crystal structure of HSA in complex with palmitic acid (PDB code 4BKE,[18] 2.35 Å). Ligand geometries were minimized using the AM1 Hamiltonian as implemented in the program Gaussian 09[26] and used as MOL2 files. Each ligand was docked in 25 independent genetic algorithm (GA) runs, and for each of these a maximum number of 100000 GA operations were performed on a single population of 50 individuals. Operator weights for crossover, mutation and migration in the entry box were used as default parameters (95, 95, and 10, respectively), as well as the hydrogen bonding (4.0 Å) and van der Waals (2.5 Å) parameters. The position of the side chain of the experimentally observed modified residue was used to define the active-site and the radius was set to 8 Å. All crystallographic water molecules and the ligands were removed for docking. The “flip ring corners” flag was switched on, while all the other flags were off. The GOLD scoring function was used to rank the ligands in order to fitness.

Building of the *apo*-Serum Albumin Models

The Phyre2 homology modelling web server was used to model the three-dimensional structure of serum albumin from rat, rabbit, porcine and sheep.[27] The coordinates of the crystallographically determined HSA (PDB code 1ETB,[28] 1.8 Å, chain A) was chosen as the main template for building the

model. The resulting protein structures had a 73%, 76%, 75% and 75% sequence identity and 95% of its sequence was modelled with 100% confidence by the template (Figure S2).

Molecular Dynamics Simulations

(a) Ligand minimization. The ligand geometries of the highest score solution obtained by docking were minimized using a restricted Hartree–Fock (RHF) method and a 6–31G(d) basis set, as implemented in the ab initio program Gaussian 09. Partial charges were derived by quantum mechanical calculations using Gaussian 09,[26] as implemented in the R.E.D. Server (version 3.0),[29] according to the RESP[30] model. Ligand coordinates obtained by docking were employed as starting point for MD simulations. The missing bonded and non-bonded parameters were assigned, by analogy or through interpolation, from those already present in the AMBER[31] database (GAFF[32]).

(b) Generation and minimization of the complexes. Simulations of the **CPF**/HSA complexes were carried out using the enzyme geometries in PDB code 4BKE[18]. Computation of the protonation state of titratable groups at pH 7.0 was carried out using the H^{++} Web server.[33] Addition of hydrogen and molecular mechanics parameters from the ff14SB[34] and GAFF force fields, respectively, were assigned to the protein and the ligands using the LEaP module of AMBER Tools 15.[35] As a result of this analysis: (i) His535 was protonated in δ position; (ii) His3, His9, His39, His146, His242, His288, His440, His464 and His510 were protonated in ε position; (iii) His67, His105, His128, His247, His338 and His367 were protonated in δ and ε positions. The protein was immersed in a truncated octahedron of ~25000 TIP3P water molecules and neutralized by addition of sodium ions. The system was minimized in five stages: (a) minimization of poorly unsolved residues 6, 41, 109, 170, 204, 205, 244, 276, 277, 317, 372, 396, 466, 519, 521, 538, 560, and 570 (1000 steps, first half using steepest descent and the rest using conjugate gradient); (b) minimization of the ligand (1000 steps, first half using steepest descent and the rest using conjugate gradient); (c) minimization of the solvent and ions (5000 steps, first half using steepest descent and the rest using conjugate gradient); (d) minimization of the side chain residues, waters and ions (5000 steps, first half using steepest descent and the rest using conjugate gradient); (e) final minimization of the whole system (5000 steps, first half using steepest descent and the rest using conjugate gradient). A positional restraint force of 50 kcal mol^{-1} $Å^{-2}$ was applied to not minimized residues of the protein during the stages a-c and to α carbons during the stage d, respectively.

(c) Simulations. MD simulations were performed using the pmemd.cuda_SPFP[36–38] module from the AMBER 14 suite of programs. Periodic boundary conditions were applied and electrostatic interactions were treated using the smooth particle mesh Ewald method (PME)[39] with a grid spacing of 1 Å. The cutoff distance for the non-bonded interactions was 9 Å. The SHAKE algorithm[40] was applied to all bonds containing hydrogen using a tolerance of 10^{-5} Å and an integration step of 2.0 fs. The minimized system was then heated at 300 K at 1 atm by increasing the temperature from 0 K to 300 K over 100 ps and by keeping the system at 300 K another 100 ps. A positional restraint force of 50 kcal mol^{-1} $Å^{-2}$ was applied to all α carbons during the heating stage. Finally, an equilibration of the system at constant volume (200 ps with positional restraints of 5 kcal mol^{-1} $Å^{-2}$ to α alpha carbons) and constant pressure (another 100 ps with positional restraints of 5 kcal mol^{-1} $Å^{-2}$ to α alpha carbons) were performed. The positional restraints were gradually reduced from 5 to 1 mol^{-1} $Å^{-2}$ (5 steps, 100 ps each), and the resulting systems were allowed to equilibrate further (100 ps). Unrestrained MD simulations were carried out for 100 ns. System coordinates were collected every 10 ps for further analysis. The molecular graphics program PyMOL[41] was employed for visualization and depicting ligand/protein structures. The cpptraj module in AMBER 14 was used to analyse the trajectories and to calculate the root-mean-square deviations (rmsd) of the protein during the simulation.[42]

MM/PBSA Calculations. The binding free energies for **CPF** on binding sub-domains IIIA and IIIB were calculated by the MM/PBSA[23] approach implemented in Amber Tools 1.5 ante-MMPBSA.py module was used to create topology files for the complex, protein and ligands and binding free energies were calculated with the MMPBSA.py module.[43] A single trajectory approach was used to calculate binding free energies considering only: (a) for 100 ns simulations, the last 80 ns (401 snapshots) of the whole MD trajectories; (b) for 150 or 200 ns simulations, the last 100 ns (401 snapshots) of the whole MD trajectories. The Poisson-Boltzmann (PB) and Generalized Born (GB) implicit solvation models were employed. The latter model provided relative free energy values more in agreement with the experimental results.

Conflicts of interest

There are no conflicts to declare.

Acknowledgements

Financial support by Spanish Ministry of Economy and Competiveness (CTQ2016-78875-P, SAF2016-75638-R and BES-2014-069404), Generalitat Valenciana (PROMETEO2017/075), Consellería de Cultura, Educación e Ordenación Universitaria (Centro singular de investigación de Galicia accreditation 2016-2019, ED431G/09) and European Regional Development Fund (ERDF) is acknowledged. This work was also supported by Instituto de Salud Carlos III (ISCIII) co-funded by Fondo Europeo de Desarrollo Regional – FEDER for the Thematic Networks and Co-operative Research Centres: ARADyAL (RD16/0006/0030). EL thanks the Xunta de Galicia for his postdoctoral fellowship. We are also grateful to the Centro de Supercomputación de Galicia (CESGA) for use of the Finis Terrae II supercomputer. The proteomic analysis was performed in the proteomics facility of SCSIE University of Valencia that belongs to ProteoRed PRB2-ISCIII and is

supported by grant PT13/0001, of the PE I+D+I 2013–2016, funded by ISCIII and FEDER.

Notes and references

‡ Abbreviations: SAs, serum albumin(s); HSA, human serum albumin; BSA, bovine serum albumin; PSA, pig serum albumin; RbSA, rabbit serum albumin; RtSA, rat serum albumin; SSA, sheep serum albumin; **CPF**, (*S*)-carprofen; IBU, (*S*)- ibuprofen.

1 D. Limones-Herrero, R. Pérez-Ruiz, E. Lence, C. González-Bello, M. A. Miranda, and M. C. Jiménez, *Chem. Sci*., 2017, **8**, 2621–2628.

2 a) W. M. O'Brien, and G. F. Bagby, *Pharmacotherapy,* 1987, **7**, 16–24; b) S. L. Curry, S. M. Cogar, and J. L. Cook, *J. Am. Anim. Hosp. Asoc*., 2005, **41**, 298-309; c) P. Lees, M. F. Landoni, J. Giraudel, and P. L. Toutain, *J. Veter. Pharmacol. Therap*., 2004, **27**, 479-490.

3 a) T. J. Peter, *All about albumin: biochemistry, genetics and medical applications*, Academic press, California, 1996; b) U. Kragh-Hansen, *Pharmacol Rev.,* 1981, **33**, 17–53.

4 X. M. He, and D. C. Carter, *Nature,* 1992, **358**, 209–215.

5 a) G. Sudlow, D. J. Birkett, and D. N. Wade, *Mol. Pharmacol*., 1975, **11**, 824–832. c) U. Kragh-Hansen, V. T. G. Chuang, and M. Otagiri, *Biol. Pharm. Bull.,* 2002, **25**, 695–704.

6 a) G. Sudlow, D. J.Birkett, and D. N. Wade, *Mol. Pharmacol*. 1976, **12**, 1252–1261; b) M. Fasano, S. Curry, E. Terreno, M. Galliano, G. Fanali, P. Narciso, S. Notari, and P. Ascenzi, *IUBMB Life,* 2005, **57**, 787–796.; c) D. C. Carter, and J. X. Ho, *Advances in protein Chemistry,* 1994, **45**, 153–203.

7 a) T. Kosa, T. Maruyama, and M. Otagiri, *Pharm. Res*., 1997, **14**, 1607–1612. b) A. F. Aubry, N. Markoglou, and A. McGann, *Comp. Biochem. Physiol. C,* 1995, **112**, 257–266. c) M. H. Rahman, T. Maruyama, T. Okada, K. Yamasaki, and M. Otagiri, *Biochem Pharmacol.,* 1993, **46**, 1721–1731. d) H. Kohita, Y. Matsushita, and I. Moriguchi, *Chem. Pharm. Bull.,* 1994, **42**, 937–940.

8 a) I. Vayá, R. Pérez-Ruiz, V. Lhiaubet-Vallet, M. C. Jiménez, and M. A. Miranda, *Chem. Phys. Lett.,* 2010, **486**, 147–153. b) V. Lhiaubet-Vallet, Z. Sarabia, F. Boscá, and M. A. Miranda, *J. Am. Chem. Soc*., 2004, **126**, 9538–9539. c) V. Lhiaubet-Vallet, F. Bosca, and M. A. Miranda, *J. Phys. Chem. B,* 2007, **111**, 423–431.

9 a) M. H. Rahman, T. Maruyama, T. Okada, K. Yamasaki, and M. Otagiri, *Biochem. Pharmacol*., 1993, **46**, 1721–1731. b) M. H. Rahman, T. Maruyama, T. Okada, T. Imai, and M. Otagiri, *Biochem. Pharmacol.,* **1993**, **46**, 1733–1740.

10 a) M. Divkovic, C. K. Pease, G. F. Gerberick, and D. A. Basketter, *Contact Dermatitis,* 2005, **53**, 189–200. b) G. Johannesson, S. Rosqvist, C. H. Lindh, H. Welinder, and B. A. G. Jönsson, *Clin. Exp. Allergy,* 2001, **31**, 1021–1030. c) A. Lahoz, D. Hernández, M. A. Miranda, J. Pérez-Prieto, I. Morera, and J. Castell, *Chem. Res. Toxicol.,* 2001, **14**, 1486–1491.

11 P. Jones, *In vitro* phototoxicity assays, in Principles and Practice of Skin Toxicology, (R. Chilcott, S. Price Eds.), John Wiley & Sons, 2008, p. 169.

12 a) Y. Merot, M. Harms, and J.-H. Saurat, *Dermatologica,* 1983, **166**, 301–307. b) H. Kietzmann, T. H., Rüther, and B. Scheuer, *Akt. Dermatol*., 1984, **10**, 17–20. c) E. Hoting, and K. H. Schultz, *Dermatosen,* 1984, **32**, 215–217. d) R. Roelandts, *Dermatologica,* 1986, **172**, 64–65, d) F. Bosca, M. L. Marin, and M. A. Miranda, *Photochem. Photobiol*., 2001, **74**, 637-655; e) A. C. Kerr, F. Muller, J. Ferguson, and R. S. Dawe, *British J. Dermatol*., 2008, **159**, 1303–1308.

13 J. Moser, F. Boscá, W. W. Lovell, J. V. Castell, M. A. Miranda, and A. Hye, *J. Photochem. Photobiol. B.,* 2000, **58**, 13–19.

14 P.-L. Toutain, A. Ferran, A. Bousquet-Mélou, Species Differences in Pharmacokinetics and Pharmacodynamics in Handbook of Experimental Pharmacology, Vol. 199, Comparative and Veterinary Pharmacology, F. Cunningan, J. Elliot, P. Lees Eds., Springer-Verlag, Berlin, Heidelberg, 2010.

15 F. Bosca, S. Encinas, P. F. Heelis, and M. A. Miranda, *Chem. Res. Toxicol*., 1997, **10**, 820–827.

16 B. Sekula, A. Ciesielska, P. Rytczak, M. Koziołkiewicz, and A. Bujacz, *Bioscience Reports,* 2016, **36**, e00338. doi: 10.1042/BSR20160089.

17 http://www.ccdc.cam.ac.uk/solutions/csd-discovery/components/gold/

18 A. Sivertsen, J. Isaksson, H. S. Leiros, J. Svenson, J. Svendsen, and B. O. Brandsdal, *BMC Struct. Biol.,* 2014, **14**, 4.

19 R. Pérez-Ruiz, E. Lence, I. Andreu, D. Limones-Herrero, C. González-Bello, M. A. Miranda, and M. C. Jiménez, *Chem. Eur. J.,* 2017, **23**, 13986–13994.

20 V. Lhiaubet-Vallet, F. Boscá, and M. A. Miranda, *J. Phys. Chem.* B, 2007, **111**, 423−431.

21 J. Ghuman, P. A. Zunszain, I. Petitpas, A. A. Bhattacharya, M. Otagiri, and S. Curry, *J. Mol. Biol.,* 2005, **353**, 38−52.

22 S. Curry, H. Mandelkow, P. Brick, and N. Franks, *Nat. Struct. Biol.,* 1998, **5**, 827–835.

23 B. R. Miller III, T. D. McGee Jr., J. M. Swails, N. Homeyer, H. Gohlke, and A. E. Roitberg, *J. Chem. Theory Comput.,* 2012, **8**, 3314−3321.

24 Z. M. Wang, J. X. Ho, J. R. Ruble, J. Rose, F. Rüker, M. Ellenburg, R. Murphy, J. Click, E. Soistman, L. Wilkerson, and D. C. Carter, *Biochim. Biophys. Acta,* 2013, **1830**, 5356−5374.

25 P. A. Zunszain, J. Ghuman, T. Komatsu, E. Tsuchida, and S. Curry, *BMC Struct. Biol.,* 2003, **3**, 6–14.

26 M. J. Frisch, G. W. Trucks, H. B. Schlegel, G. E. Scuseria, M. A. Robb, J. R. Cheeseman, G. Scalmani, V. Barone, B. Mennucci, G. A. Petersson, H. Nakatsuji, M. Caricato, X. Li, H. P. Hratchian, A. F. Izmaylov, J. Bloino, G. Zheng, J. L. Sonnenberg, M. Hada, M. Ehara, K. Toyota, R. Fukuda, J. Hasegawa, M. Ishida, T. Nakajima, Y. Honda, O. Kitao, H. Nakai, T. Vreven, J. A. Montgomery, Jr., J. E. Peralta, F. Ogliaro, M. Bearpark, J. J. Heyd, E. Brothers, K. N. Kudin, V. N. Staroverov, R. Kobayashi, J. Normand, K. Raghavachari, A. Rendell, J. C. Burant, S. S. Iyengar, J. Tomasi, M. Cossi, N. Rega, J. M. Millam, M. Klene, J. E. Knox, J. B. Cross, V. Bakken, C. Adamo, J. Jaramillo, R. Gomperts, R. E. Stratmann, O. Yazyev, A. J. Austin, R. Cammi, C. Pomelli, J. W. Ochterski, R. L. Martin, K. Morokuma, V. G. Zakrzewski, G. A. Voth, P. Salvador, J. J. Dannenberg, S. Dapprich, A. D. Daniels, Ö. Farkas, J. B. Foresman, J. V. Ortiz, J. Cioslowski, and D. J. Fox, Gaussian 09, Revision A.2, Gaussian, Inc.: Wallingford CT, 2009.

27 L. A. Kelley, S. Mezulis, C. M. Yates, M. N. Wass, and M. J. E. Sternberg, *Nature Protocols,* 2015, **10**, 845−858.

28 J. A. Hamilton, L. K. Steinrauf, B. C. Braden, J. Liepnieks, M. D. Benson, G. Holmgren, O. Sandgren, and L. Steen, *J. Biol. Chem.,* 1993, **268**, 2416−2424.

29 a) E. Vanquelef, S. Simon, G. Marquant, E. Garcia, G. Klimerak, J. C. Delepine, P. Cieplak, and F.-Y. Dupradeau, *Nucleic Acids Res.,* 2011, **39**, W511−W517. b) http://upjv.q4md-forcefieldtools.org/RED/ (accessed June 1, 2018). c) F.-Y. Dupradeau, A. Pigache, T. Zaffran, C. Savineau, R. Lelong, N. Grivel, D. Lelong, W. Rosanski, and P. Cieplak, *Phys. Chem. Chem. Phys.,* 2010, **12**, 7821−7839.

30 W. D. Cornell, P. Cieplak, C. I. Bayly, I. R. Gould, K. M. Merz, D. M. Ferguson, D. C. Spellmeyer, T. Fox, J. W. Caldwell, and P. A. Kollman, *J. Am. Chem. Soc.,* 1995, **117**, 5179−5197.

31 D. A. Case, T. E. Cheatham, T. Darden, H. Gohlke, R. Luo, K. M. Merz, O. Onufriev, C. Simmerling, B. Wang, and R. J. Woods, *J. Comput. Chem.,* 2005, **26**, 1668–1688.

32 a) J. Wang, R. M. Wolf, J. W. Caldwell, P. A. Kollman, and D. A. Case, *J. Comp. Chem.,* 2004, **25**, 1157–1174. b) J. Wang, W. Wang, P. A. Kollman, and D. A. Case, *J. Mol. Graphics Modell.,* 2006, **25**, 247–260.

33 a) J. C. Gordon, J. B. Myers, T. Folta, V. Shoja, L. S. Heath, and A. Onufriev, *Nucleic Acids Res.,* 2005, **33** (Web Server issue):W368. b) http://biophysics.cs.vt.edu/H++.

34 J. A. Maier, C. Martinez, K. Kasavajhala, L. Wickstrom, K. E. Hauser, and C. Simmerling, *J. Chem. Theory Comput.,* 2015, **11**, 3696–3713.

35 D. A. Case, J. T. Berryman, R. M. Betz, D. S. Cerutti, T. E. Cheatham III, T. A. Darden, R. E. Duke, T. J. Giese, H. Gohlke, A. W. Goetz, N. Homeyer, S. Izadi, P. Janowski, J. Kaus, A. Kovalenko, T. S. Lee, S. LeGrand, P. Li, T. Luchko, R. Luo, B. Madej, K. M. Merz, G. Monard, P. Needham, H. Nguyen, H. T. Nguyen, I. Omelyan, A. Onufriev, D. R. Roe, A. Roitberg, R. Salomon-Ferrer, C. L. Simmerling, W. Smith, J. Swails, R. C. Walker, J. Wang, R. M. Wolf, X. Wu, D. M. York, P. A. Kollman, AMBER 2015, University of California, San Francisco, 2015.

36 A. W. Goetz, M. J. Williamson, D. Xu, D. Poole, S. Le Grand, and R. C. Walker, *J. Chem. Theory Comput.,* 2012, **8**, 1542–1555.

37 R. Salomon-Ferrer, A. W. Goetz, D. Poole, S. Le Grand, and R. C. Walker, *J. Chem. Theory Comput*., 2013, **9**, 3878–3888.

38 S. Le Grand, A. W. Goetz, and R. C. Walker, *Comp. Phys. Comm.,* 2013, **184**, 374–380.

39 T. A. Darden, D. York, and L. G. Pedersen, *J. Chem. Phys.,* 1993, **98**, 10089–10092.

40 J.-P. Ryckaert, G. Ciccotti, and H. J. C. Berendsen, *J. Comput. Phys.,* 1977, **23**, 327–341.

41 W. L. DeLano, The PyMOL Molecular Graphics System. (2008) DeLano Scientific LLC, Palo Alto, CA, USA. http://www.pymol.org/ .

42 D. R. Roe, and T. E. Cheatham, *J. Chem. Theory Comput.,* 2013, **9**, 3084–3095.

43 http://www.amber.utah.edu/AMBER-workshop/London-2015/pca/

Toc Graphic

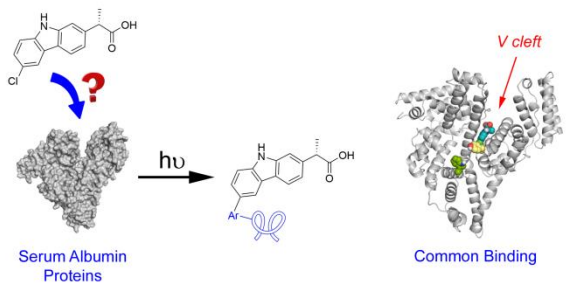

Photoreactivity, proteomic and molecular dynamic simulation studies demonstrate the existence of a common recognition center for carprofen in serum albumins of different species, in the interface between subdomains IB and IIIA.